BROADBAND FIBER BRAGG GRATING INTERROGATION FOR STRUCTURAL HEALTH MONITORING

Richard J. Black, Joannes M. Costa, Behzad Moslehi, Ronak Patel, Vahid Sotoudeh
Intelligent Fiber Optic Systems Corporation (IFOS)
2363 Calle del Mundo
Santa Clara, CA 95054
www.ifos.com

ABSTRACT

A structural health monitoring (SHM) system with interrogation nodes each supporting up to 256 fiber Bragg grating (FBG) sensors for a ±500 microstrain strain range per sensor is described. Each interrogation node supports 16 subsections with all sensors within a subsection interrogated simultaneously at sampling rates ranging from kHz to MHz. The architecture can be scaled to support over 2000 sensors. A cantilever beam test article with 15 sensors having strain resolution of better than 0.1 microstrain for 6 kHz sampling is demonstrated. Acoustic emission detection is demonstrated with a MHz sampling rate version of the interrogator.

1. INTRODUCTION

Fiber optic (FO) sensor systems are providing new and effective measurements in a multitude of applications benefiting from the following FO properties:

(1) immunity to electromagnetic interference (EMI) – of importance in many applications particularly the high EMI environments in naval systems

(2) electromagnetic compatibility (EMC) since fibers do not radiate EM energy

(3) electrical passivity and thus safety in explosive environments

(4) low weight – of particular importance in aerospace applications

(5) small dimensions allowing:

   a. integration into (i) very small dimensional spaces and (ii) smart materials including composites with minimum creation of voids

   b. access through small key holes and access points

(6) transmission capability over long distances (many kilometers)

(7) high durability in many environments including marine, extreme temperature, high pressure and high radiation environments

SAMPE Conference Proceedings. Baltimore, MD, May 18-21, 2015. Society for the Advancement of Material and Process Engineering.

(8) capacity for installation with less labor than comparable electronic sensors – instead of the multiple wires required for electronic sensors, a single optical fiber cable can support many multiplexed sensors with no local power requirement

Fiber Bragg Gratings (FBGs) [1] form the prime example of a sensor that lends itself to multiplexing along a single optical fiber. In an end-to-end FBG sensor system [2, 3], an FBG interrogator [4-6] supports FBGs that can:

(1) form multiple sensors on one or multiple optical fibers simultaneously through wavelength division and other multiplexing techniques

(2) provide information regarding the dynamic strain and temperature (or derivative measurands) seen by the FBGs, through measurement of characteristic wavelengths

(3) provide a basis for monitoring structural loading and health state

FBG sensing systems are being deployed in a wide variety of structural health monitoring (SHM) applications [7-14] with the measurement of parameters such as strain, temperature [15], fracture, vibration [16], or simultaneously sensing multiple parameters. Diverse applications include shipping (stress corrosion crack monitoring [17], propeller blades [18], masts and sails [19], trimarans [20], fast naval vessels [21]), aerospace (airframes / aircraft wings [8, 22-24], jet engines [7, 25], thermal protection systems [15, 26-28]), space [29], robotics [30], nuclear reactors [31], wind turbines [8] [32-34], concrete structures [5, 35], bridges [10, 12, 36], MRI compatible medical devices [37, 38], oil & gas [39-41] and geothermal wells [42]. Challenges in implementation of fiber optic sensing systems include: (a) scalability, and (b) interconnection (ingress/egress [43-45]) and cabling.

In Section 2, we discuss a scalable interrogation system architecture. Following that, in Section 3, we provide examples of low frequency strain monitoring on a cantilever beam (up to 6 kHz sampling), and, in Section 4, high frequency acoustic emission (AE) monitoring, before, in Section 5, concluding with comments on application to large structures such as ships (on a fleet-wide basis and/or aircraft).

2. SENSOR INTERROGATION SYSTEM ARCHITECTURE

In Figure 1, we show the IFOS FBG interrogation network with a scalable architecture for supporting up to 2048 sensors based on multiple interrogation nodes, each supporting up to 256 FBG sensors with an independent strain range per sensor of over ±500 microstrain. Each interrogation node can support 4 fibers with up to 64 sensors per fiber with the sensors being wavelength division multiplexed over 154 nm achieved by partial use of 4 wavelength bands (S, C, L and U) with up to 16 sensor wavelengths per band. These 16 sensors can be examined simultaneously at a sampling rate determined by the digital post-detection electronics shown in Figure 2. Note that Figure 2, which provides a functional diagram of the interrogator nodes, is neither to scale nor representative of the actual 3D physical positions of the subsystems. If a larger strain range is desired then the number of sensors is reduced as shown in Figure 3. For

example, for ±1500 microstrain per sensor, the design allows support of up to 8 sensors per band and 32 sensors per fiber, 128 sensors per interrogation node and 1024 per 8-node system.[1]

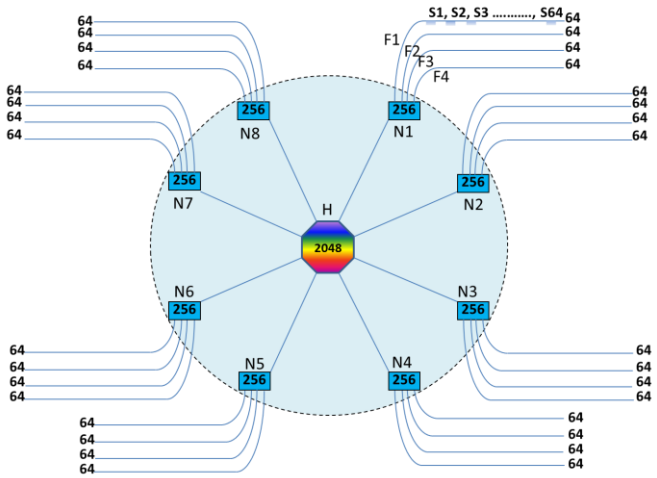

Figure 1: Scalable sensor network architecture supporting up to 2048 grating sensors based on up to 8 networked interrogation nodes (N1, …, N8) connected through a central gigabit Ethernet hub (H). Each node supports up to 256 sensors distributed among 4 optical fibers (F1, …, F4) per node with up to 64 grating-based sensors (G1, …, G64) per fiber assuming a strain range of ±500 microstrain per sensor. The nodes can be either contained in a single box or distributed over the structure.

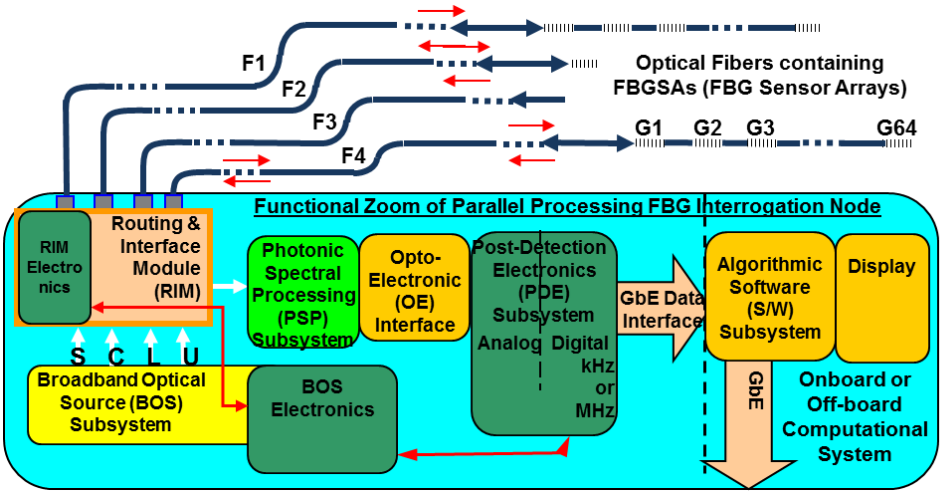

Figure 2: Functional schematic of building block interrogation node including photonic, electronic and software/firmware subsystems and modules.

[1] Note that keeping the FBGs separated in wavelength so as to avoid cross-talk means that the relationship is not linear, i.e., for 256 sensors we have only ±500 microstrain rather than ±1500/2 microstrain. Nevertheless, we have found that ±500 microstrain is very adequate for test objects developed such as a cantilever beam.

The number of sensors can be increased if a smaller range of strain values is required example, each fiber can support 64 sensors and each node can support 256 sensors at ±500 microstrain (Figure 3) resulting in support for 2048 sensors in the 8-module networked configuration

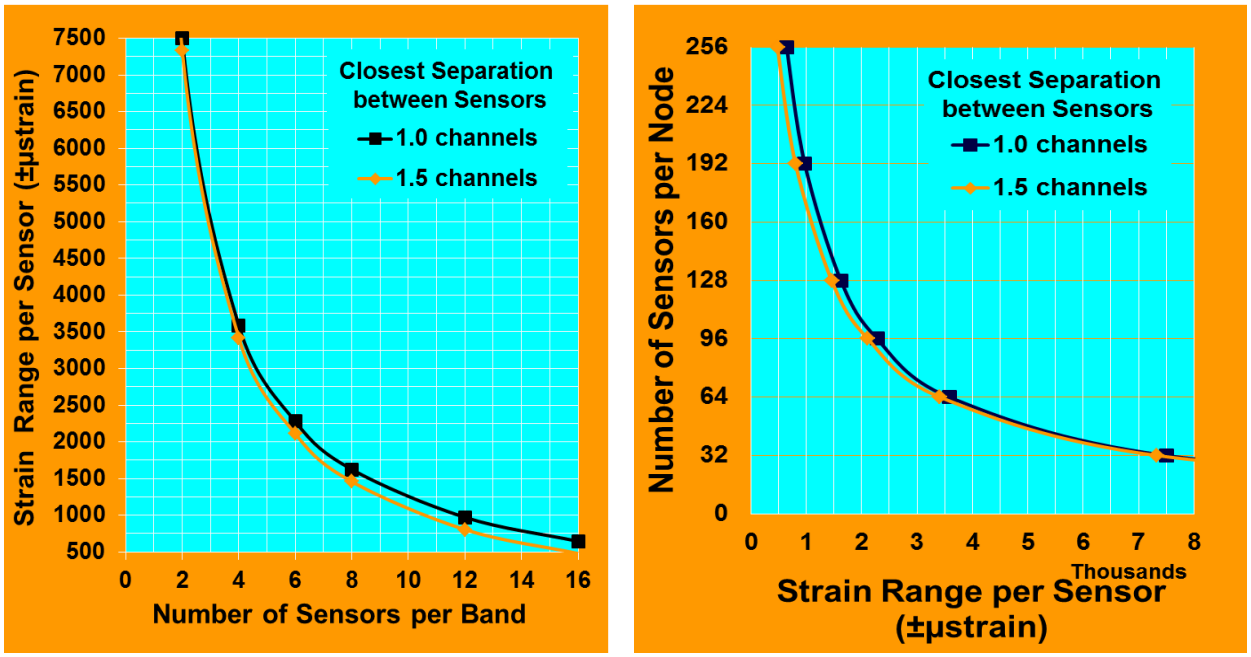

Figure 3: Number of sensors supported dependent on strain range given when each wavelength band is divided into 48 channels separated by approximately 0.8 nm: (a) ± strain range per sensor as a function of number of sensors per wavelength band. (b) Number of sensors per interrogation node as a function of ± strain range per sensor.

3. LOW TO MODERATE FREQUENCY MONITORING: CANTILEVER BEAM RESULTS

3.1 Cantilever Beam Sensor Layout

The cantilever beam described in this section was used as the "work horse" test article for developing and demonstrating the features of the GUI as discussed in Sections 3.2 to 3.4. A schematic showing the sensor layout is shown in Figure 4. Note that the wavelength bands (S, C, L, and U) increase along the beam from the clamping region on the left to the tip at the right. Thus, given tip deflection, we would expect that the S band gratings closest to the clamp will see the largest strains, while relatively small strains will be seen by the U band gratings hear the tip. This expectation is borne out by the results of Section 4.

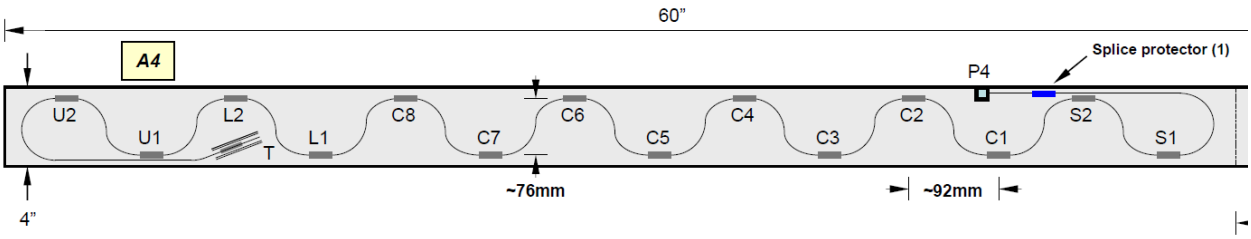

Figure 4: Design layout for sensors on cantilever beam.

Figure 5 shows a photograph of the cantilever beam (painted black) with the far end attached to a shelf with two C-clamps (one of which is seen). The beam is to the right of the monitor for the interrogator. A yellow fiber optic cable attaches the beam sensors to the interrogator and the wavelength and strain output is seen on the monitor, examples of which are detailed in Section 4.

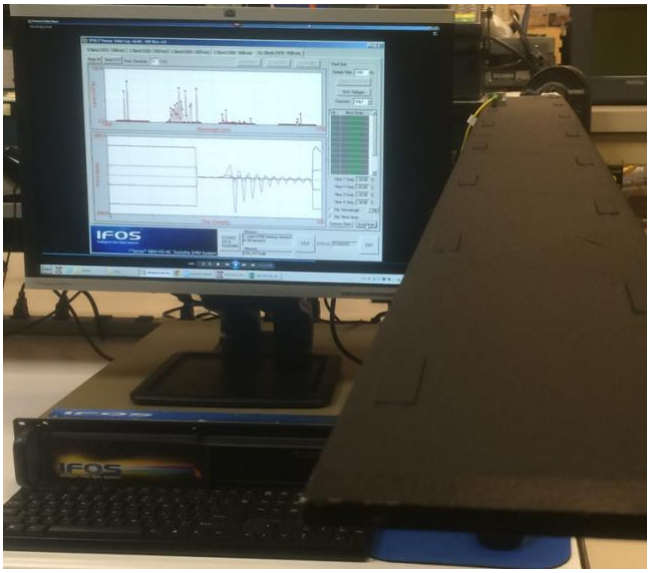

Figure 5: Interrogator (left) and cantilever beam (right).

3.2 GUI for Multiple Wavelength Bands

Figure 6 shows the interrogator graphical user interface (GUI) when a cantilever beam is set in motion and responds with a damped sinusoidal oscillation. The data captured in the GUI is for sensors with wavelengths distributed over in four optical bands (S, C, U and L from left to right in the upper plot of the GUI). Computed strains for the sensors are shown in the lower plot. The sensors closest to the attached end of the cantilever register the most strain as expected. This can be verified by examining the wavelength plots. In Figure 7, which covers a range of 220 nm with each nm corresponding to approximately 830 microstrain, we see oscillations decreasing from S (closest the clamped end of the cantilever) to C with L and U oscillations being imperceptible on that scale. Within each band, the largest wavelength is closet the calmped end and indeed, for the S-band wavelength zoom of Figure 8, we have a decrease from S1 to S2, and similarly for the C-band wavelengths in Figure 9, we see a decrease from C1 to C8.

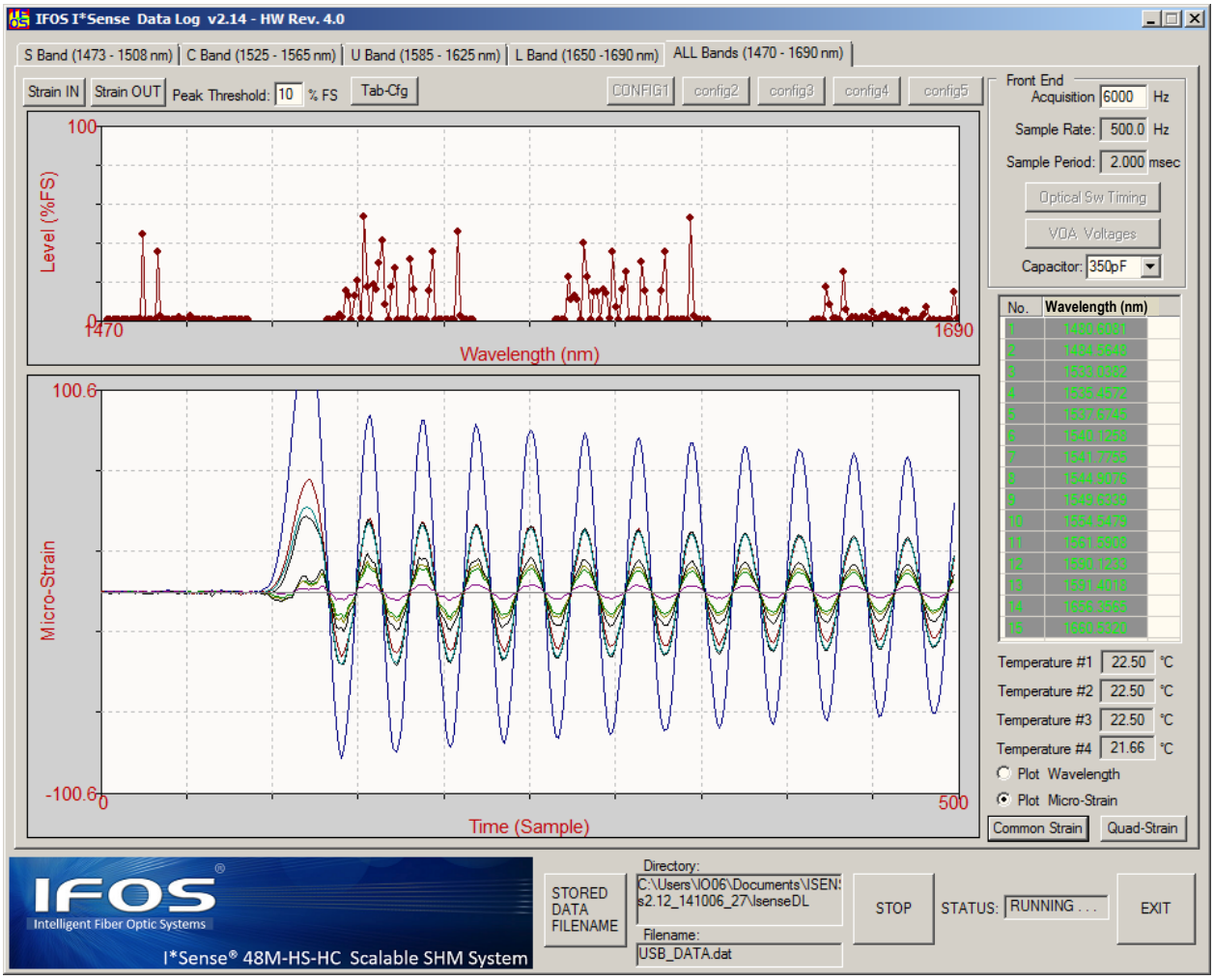

Figure 6: GUI version 2.14 showing strain variation for multiple FBGs on the cantilever beam of the previous section

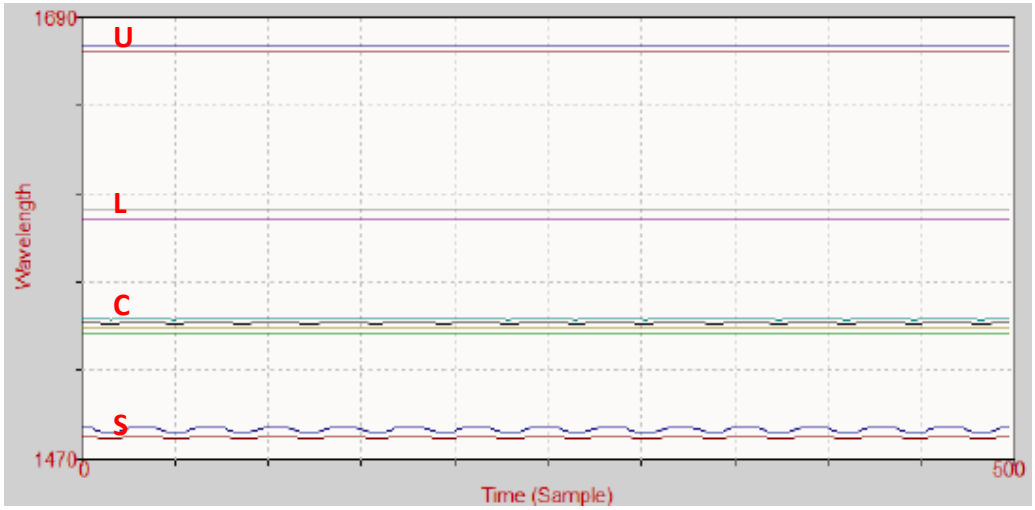

Figure 7: All band wavelength response for a large (>15”) deflection of the cantilever beam end.

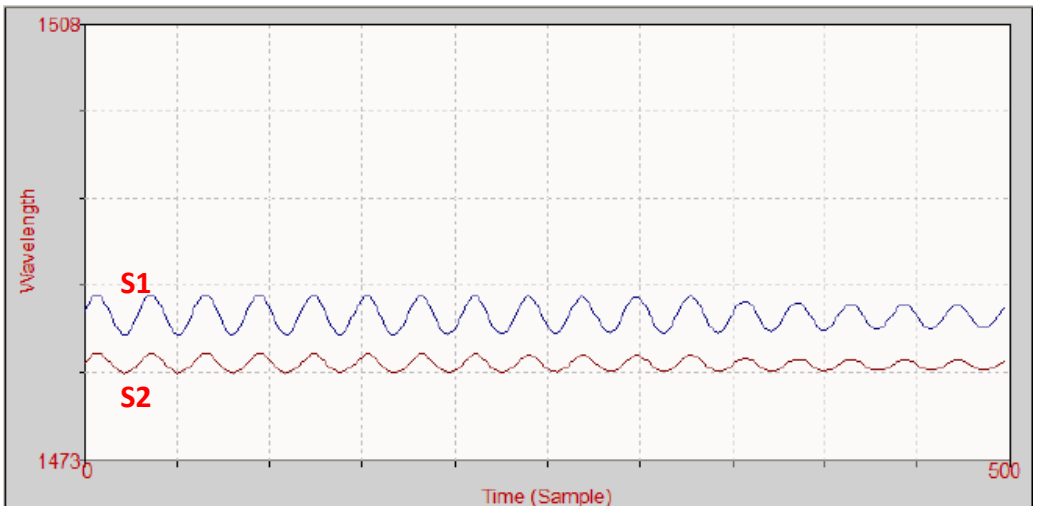

Figure 8: S band wavelength response for a large (>12") deflection of the cantilever beam end.

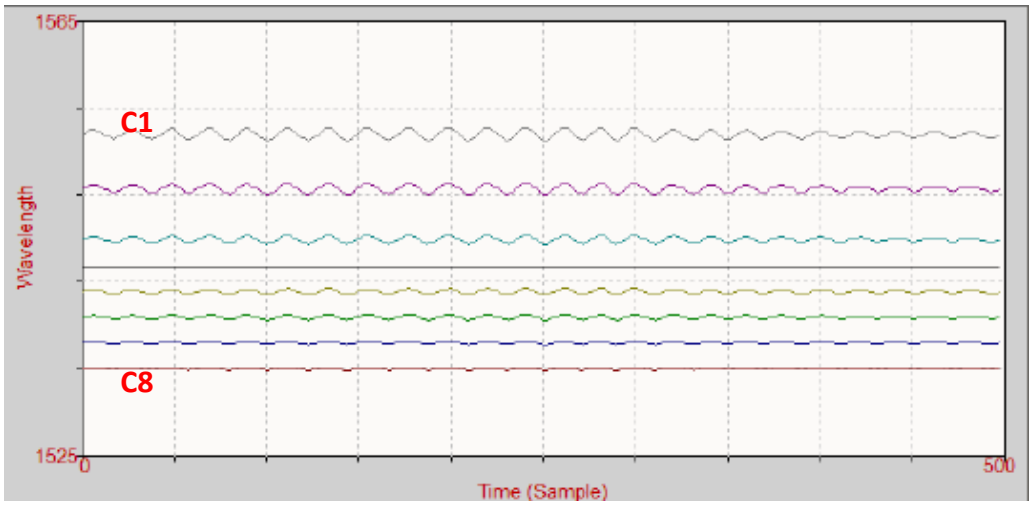

Figure 9: C band wavelength response for a large (>12") deflection of the cantilever beam end.

3.3 Larger Strain Range Example (~ 1000 microstrain)

The first two figures are similar to those of the previous section except that in this case the initial deflection of the cantilever beam was upwards (resulting in compression of the gratings on its upper side – maximum 800 microstrain), and then, while still holding the beam, the upward deflection was reduced until the strain was around -140 microstrain at 3.3 seconds before the beam was released and allowed to oscillate with its characteristic damped sinusoid. Also, in Figure 10, the tab for the C Band sensors (in the range 1528 nm to 1565 nm) was chosen and the GUI configuration files were setup to plot just 4 selected FBG sensors, although results were recorded in a file at the full acquisition rate (6000 Hz) for 9 C band sensors (8 for strain and one at the longest wavelength for temperature). Note that the upper plot simply registers the amplitudes seen by the PSP in Gaussian channels centered around 48 wavelengths each separated by 100 GHz in optical frequency corresponding to approximately 0.8 nm wavelength separation at 1550 nm. From these amplitudes, the interrogator software computes the FBG

center wavelengths with resolution that is sub-picometer (in fact close to femtometer – see next subsection) and with accuracy that is of picometer order depending on the FBG spectral details.

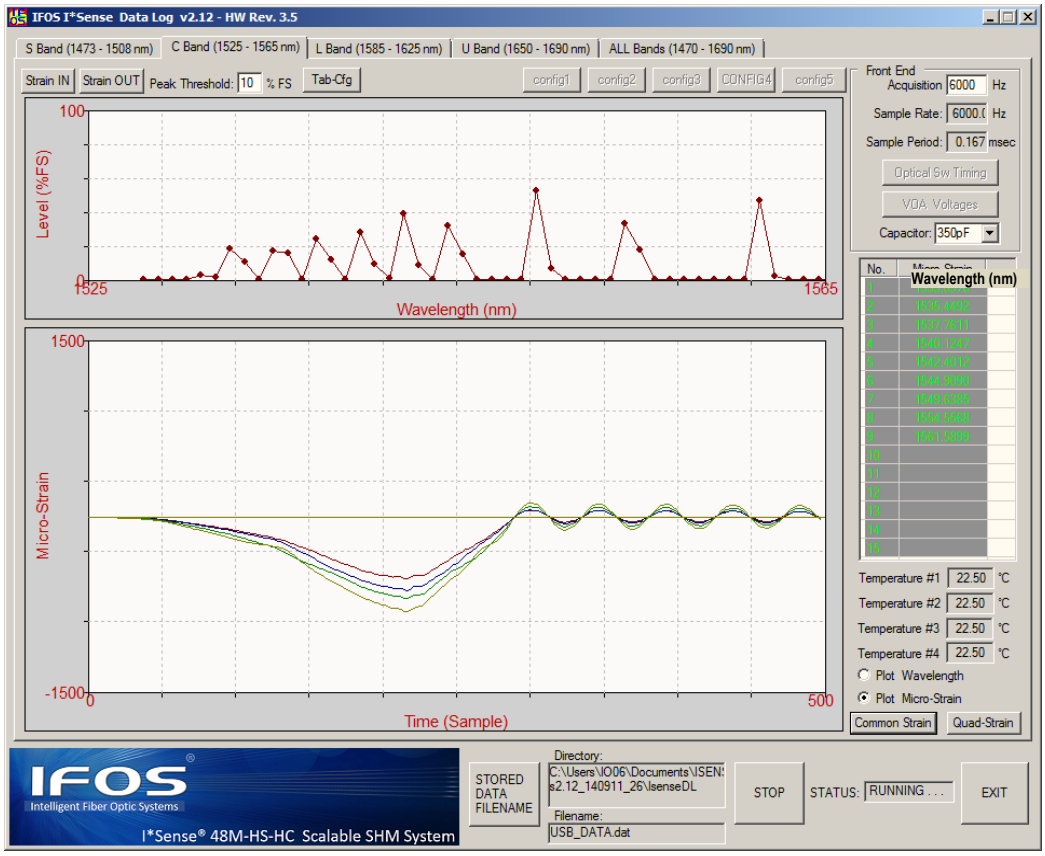

Figure 10: GUI showing a single switch state (C-band for cantilever recording at 6 kS/s) with strain for four of the sensors in the lower plot plotted live at a decimated rate.

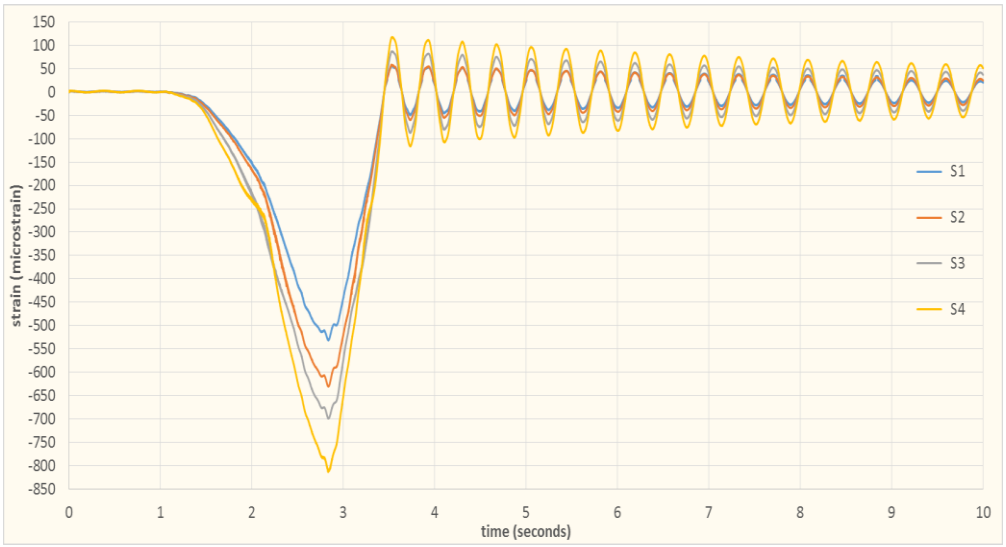

Figure 11: Data plotted from the Excel file saved using the GUI of Figure 10 plotted at 6 kS/s.

3.4 Smaller Strain Range Examples (~microstrain to sub-microstrain)

The next two plots show the excellent sensitivity of the system to small amplitude vibrations. In particular, Figure 12 shows that reasonably clean sinusoidal oscillations of the cantilever are detected down to microstrain levels (scale ±1.9 microstrain – i.e. a factor of over 500 in comparison with the previous example) when running at full speed (6 kS/s). In Figure 13, the scale is ±0.1 microstrain, i.e., over four orders of magnitude smaller than the scale in Figure 10.

Figure 12 shows a slight asymmetry (tenths of a microstrain) with the oscillations oscillating about a "zero" that is slightly lower than the zero on the graph. In addition, the oscillation amplitudes and offsets from zero microstrain are sensor dependent. This sensor-dependent offsets of the "zeros" is due to the system having been "zeroed" when there was still a very small motion of the beam.

This asymmetry effect is more evident in Figure 13, where the scale is ±0.1 microstrain. At this level the cantilever was also susceptible to vibrations from computer equipment and air conditioning on the bench to which it was attached. The experiment was simply a quick illustration of the sensitivity rather than a carefully controlled test in which all sources of environmental noise had been eliminated.

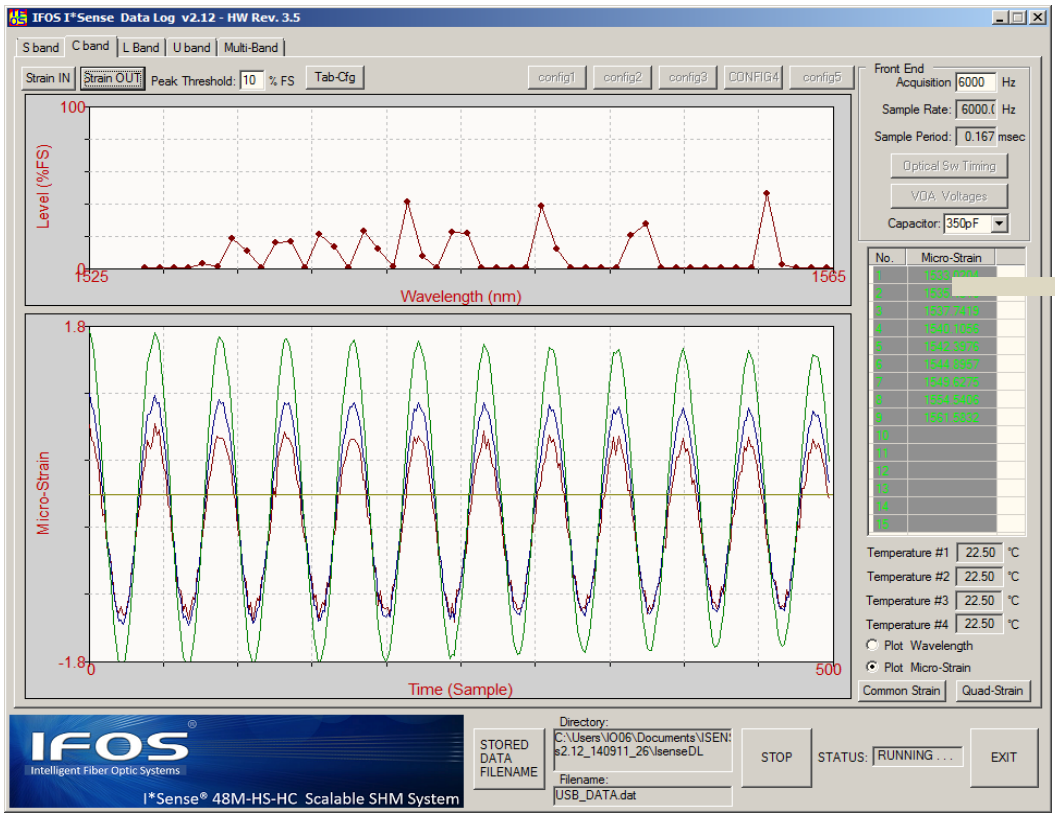

Figure 12: Reasonably clean sinusoidal oscillations of the cantilever are detected down to microstrain levels (scale ±1.9 microstrain) when running at full speed (6 kS/s).

On the other hand we do note that the noise effects in Figure 13 are nearly an order of magnitude smaller than the oscillations, i.e., on the order 0.01 microstrain (10 nanostrain) equivalent, corresponding to approximately 0.01 pm (10 fm) wavelength shifts This corresponds to our expectations for the low noise analog post-detection electronics (A-PDE) and the 20 bit, i.e. $2^{20} \approx 10^6$, resolution of the digital post-detection electronics (D-PDE) used for the 6 kS/s version of our interrogator. In particular, we expect the system to be able to resolve wavelength changes from on the order of 0.8 nm/10^6 = 0.8 fm ≈ 1 fm up to (48-1) x 0.8 nm = 37.6 nm, i.e., over 7 orders of magnitude. The lower bound is only a very rough approximation given that the conversion from wavelength shift to the output from the PSP channels is somewhat nonlinear.

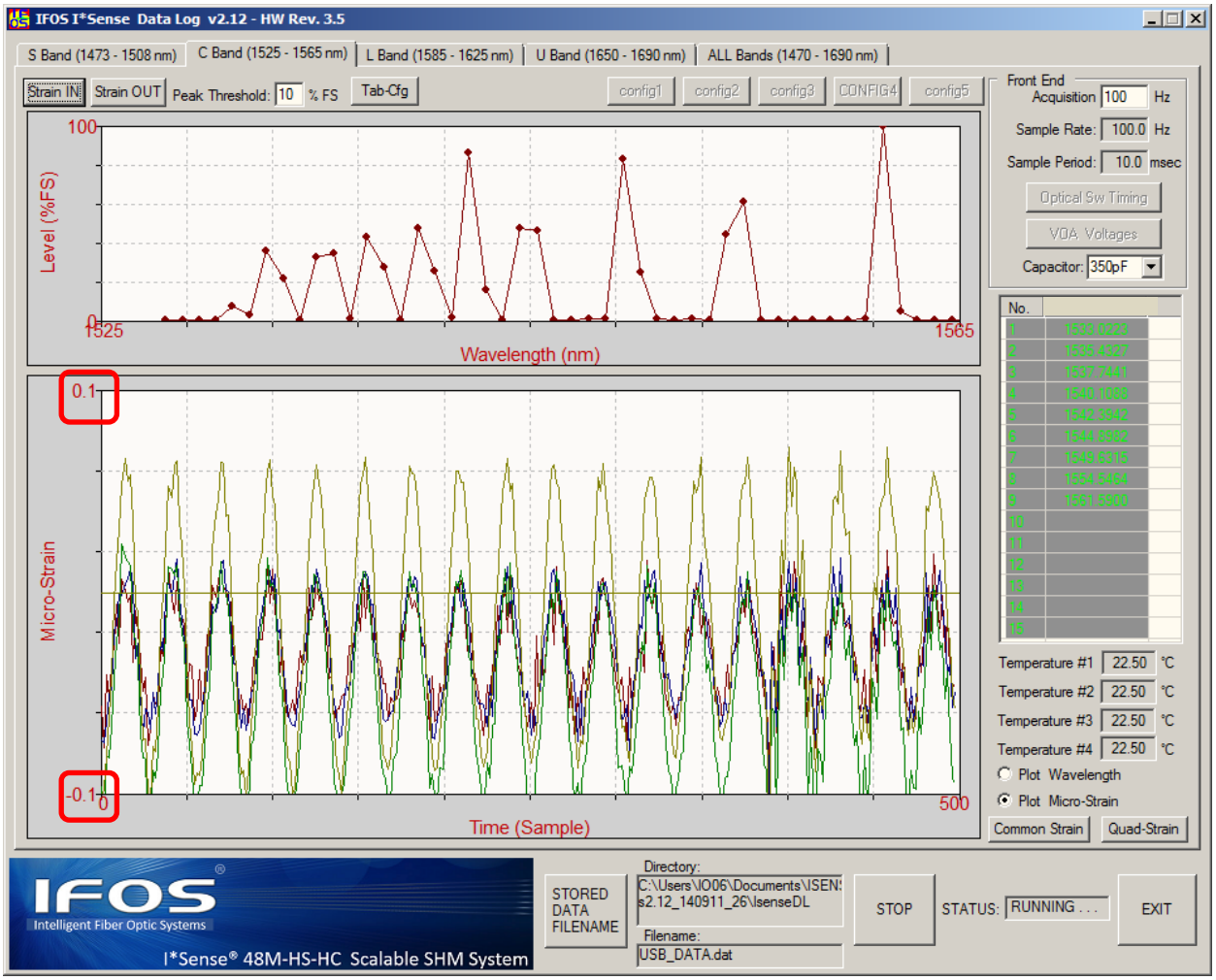

Figure 13: Strain resolution is better than 0.1 microstrain as shown with the cantilever oscillating with a very small amplitude (scale ±0.1 microstrain).

4. HIGH FREQUENCY MONITORING: ACOUSTIC EMISSIONS

Monitoring for proximity to failure is key to maximizing remaining useful life while ensuring safe operation. Acoustic emission (AE) monitoring is a reliable, non-intrusive system for the detection of damage in a range of structures. Initial work using FBGs was performed by Perez and collaborators [46]. We have developed a 1 MS/s, 16-bit, 64-channel version of the D-PDE in our interrogation system that allows simultaneous monitoring of 16 sensors at 1 MS/s (for Nyquist limited 500 kHz phenomena). Figure 16 shows the response of our 1 MS/s system using optics for 48 of the possible 64 channels for an example FBG sensor in a standard "pencil break" test on an aluminum plate, i.e., where pencil-lead breakage (PLB) was used as a reproducible artificial acoustic emission (AE) source often referred to as a Hsu-Nielsen source [47, 48]. The upper window is the 1 MHz data collector GUI (CollectBurst), which notes the event counts and wavelengths for four FBGs. It also records a file with wavelengths and filtered strains at 1 MS/s for 6000 samples, i.e., 6 ms, whenever and AE event is detected. The lower window is the EventViewer, which shows (a) the time domain responses for two of the FBGs on the left and (b) the frequency domain responses on the right with the green traces being the FFT system response before the event in the first 2 ms and the red traces being the FFT in the following 4 ms.

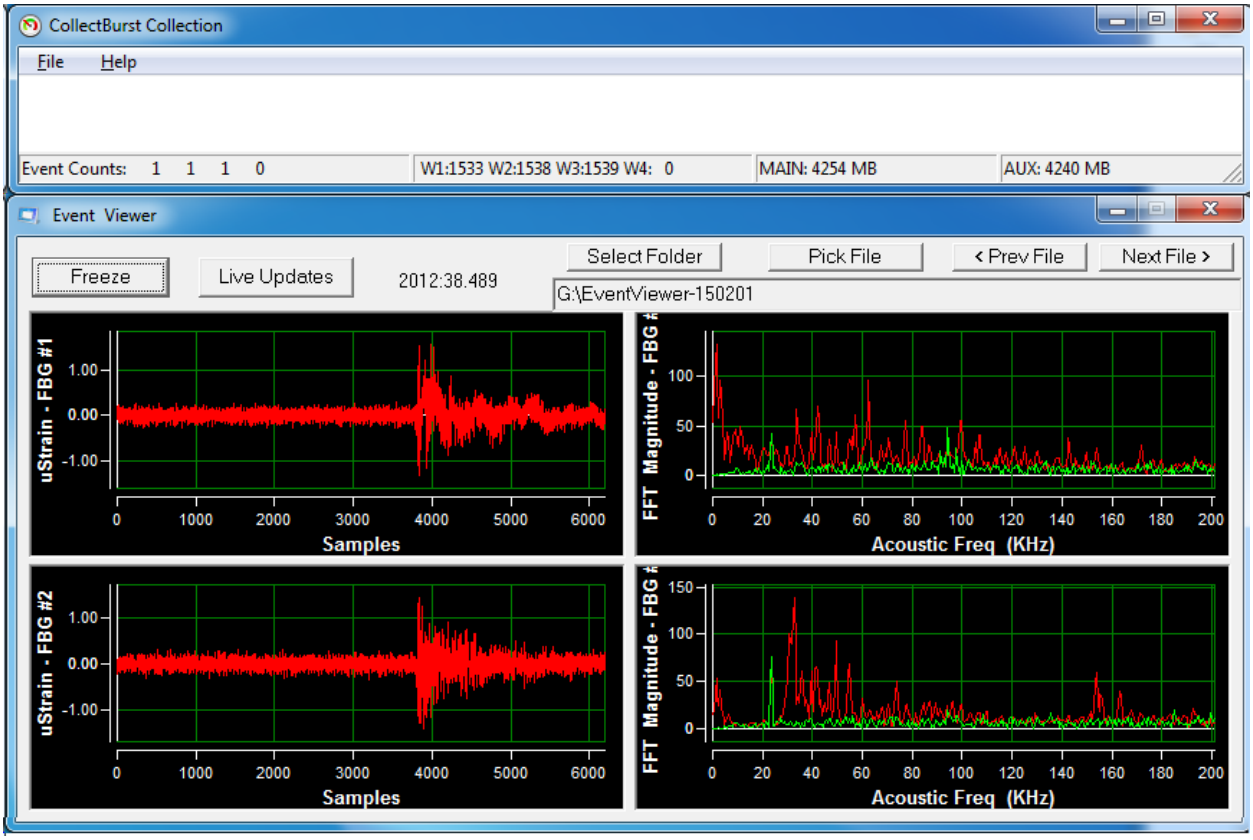

Figure 14: High-speed sampling at 1 MS/s for detection of acoustic emissions (AE) from a pencil led break.

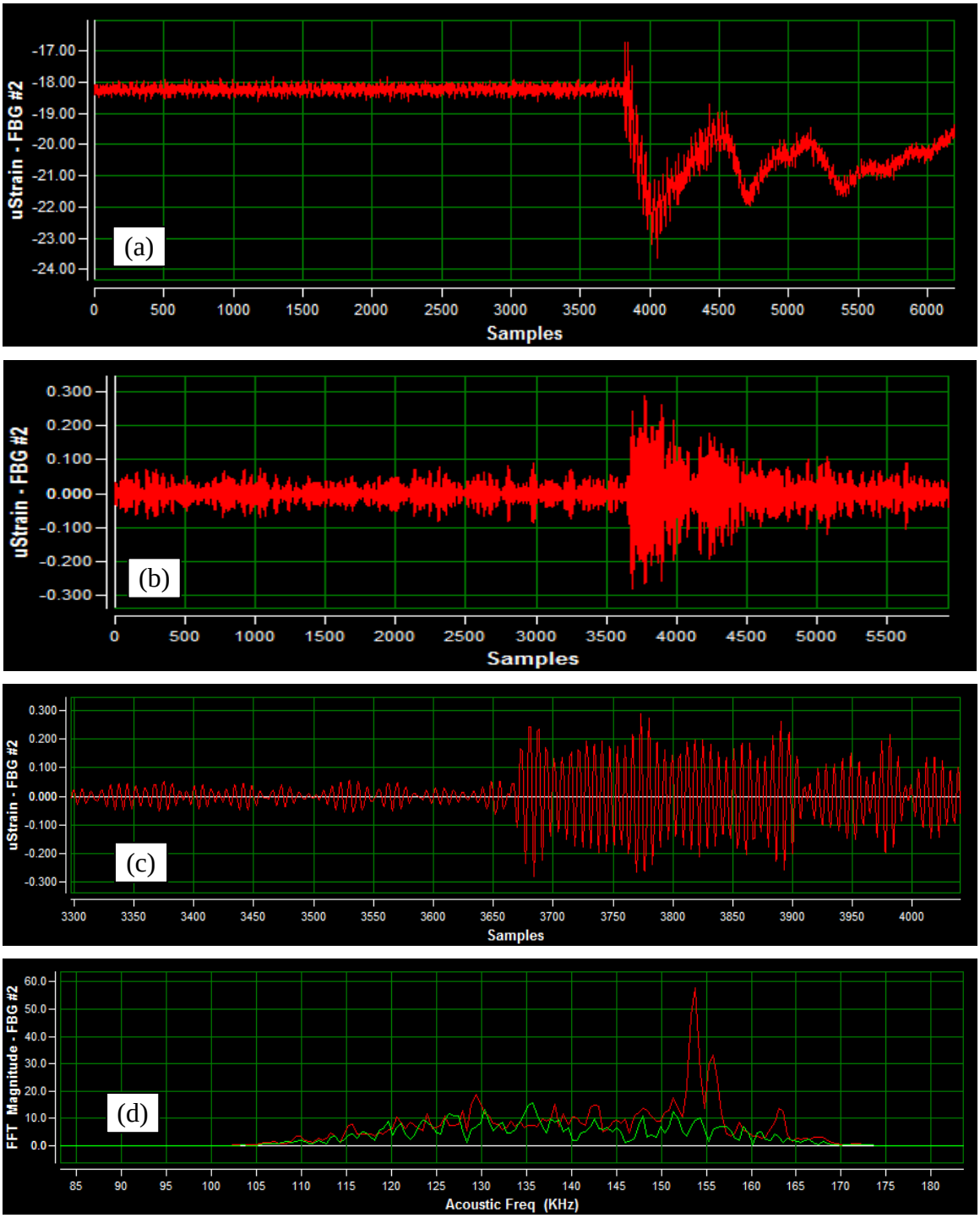

Figure 15: Same as previous figure but (a) unfiltered strain, (b) with application of a bandpass filter between 105 and 170 kHz, (c) time zoom into the region of multiple AE events, (d) comparison of pre-trigger (green) and post-trigger (red) signals in the frequency domain.

Instead of passive listening over a broad range of frequencies for AE as a precursor to cracking of a structure, one can also exploit high frequency FBG monitoring of Lamb waves actively excited by a piezoelectric actuator. In complementary work, we have used time-of-flight

measurements to determine damage position such as delamination in composites [49]. Particularly important in the time-of-flight measurements is the ability provided by our parallel processing approach to simultaneously measure the response of multiple FBGs and thus determine relative phases. For example, Figure 16(a) shows measurements from 4 FBGs at the corners of a curved composite plate given a 30 kHz pulse from a piezoelectric actuator at the center of the plate. From the different times of arrivals at the 4 FBGs, taking account of reflections from the edges of the plate as well as a delaminated area, the approximate psotion of the delamination was determined as in Figure 16(b).

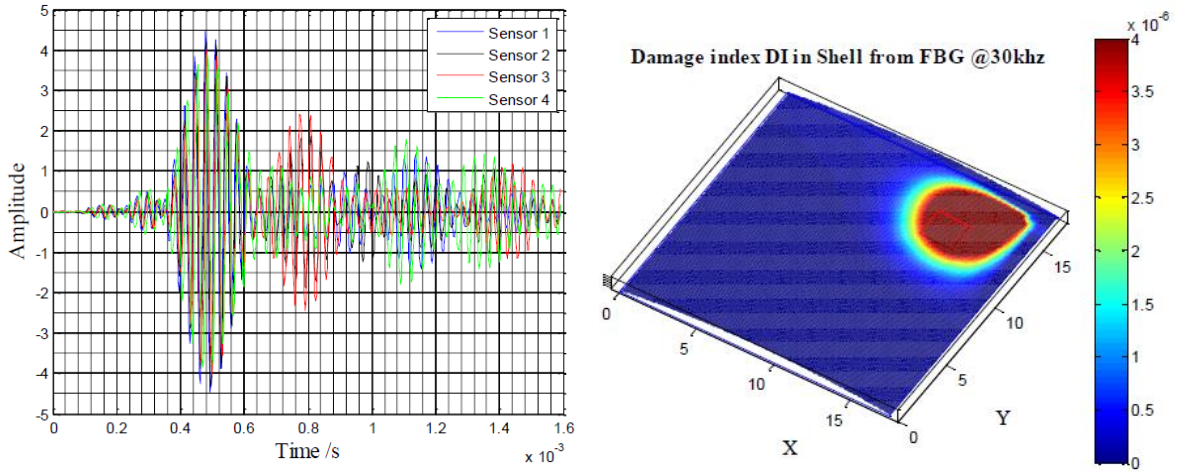

Figure 16 (a) Response signals from 4 FBG sensors at the 4 corners of a curved composite plate with excitation frequency of 30 kHz. (b) Damage Index (DI) in the composite plate deduced from time-of-flight Lamb wave measurements provided by the 4 FBGs.

As an alternative to the time-of-flight approach, with collaborators, we have also used high frequency spectral methods [50, 51] analogous to the electromagnetic impedance method [52] for damage detection.

5. CONCLUSIONS

Up to many kilometers in length, optical fibers are small-in-diameter, light-in-weight, electromagnetic-interference immune, electrically passive, chemically inert, flexible, and embeddable into different materials. They enable distributed-sensing in harsh environments requiring temperature and radiation tolerance. With appropriate processing and packaging, they can be very robust and well suited to operational demands. In this paper, we reviewed developments for a broadband (DC to MHz) multiplexed FBG array sensor systems and example application for (1) strain/load monitoring from 100s of Hz to kHz and (2) high frequency acoustic emission monitoring to MHz. This work is providing a path to a complete end-to-end fiber optic sensor system that comprises (1) ruggedized sensor interrogators, (2) scalable packaged sensors and mechanisms (one to two thousand depending on the strain range), (3) operation in harsh environments, and (4) intelligent algorithms implemented in firmware or software for decision support.

We believe that the implementation of such a system on a fleet-wide basis has the potential to provide important data to manage fleet assets, improve safety, and reduce costs for maintenance.

First, the system can provide low to moderate frequency strain/loading and vibration monitoring. Second the same sensor network can be used with high sampling rate interrogation for damage detection using methods such as acoustic emission measurement. In the latter case, a high performance (MHz) interrogator can switch between different parts of the fiber optic network on a ship and examine the substructure associated with sensors in a given wavelength band on a given fiber before the optical switch moves onto the next set of sensors within the network aboard the ship (or other structure such as an aircraft equipped with a FBG sensor network).

6. ACKNOWLEDGEMENTS

We thank Dr. Ignacio Perez, ONR Program Officer for Navy SBIR Phase II Contract N00014-11-C-0437, and his colleagues, particularly Drs. Ben Grisso, Tom Brady and Mark Seaver, for insightful comments and support. Steve Ahlport provided interrogation software/firmware support and Levy Oblea hardware support. The MHz version of the interrogator was initially supported by NASA Phase II contract NNX10RA83P with the current AE detection software developed under Navy SBIR Phase I Contract N68335-14-C-0350.

7. REFERENCES

[1] Hill, K. O. and Meltz, G. "Fiber Bragg Grating Technology Fundamentals and Overview." *J. Lightwave Technol.* 15 (1997): 1263-1276.

[2] Black, R. J. and Moslehi, B. "Advanced end-to-end fiber optic sensing systems for demanding environments (Invited Paper)." *Proc. SPIE 7817*. San Diego, CA, 2010. International Society for Optics and Photonics—pp. 0L.1-9.

[3] Moslehi, B. and Black, R. J. "Knowledge Generation Employing Multi-functional Photonically Sensorized Environments (Plenary Talk)." *Proc. 1st International Applied Photonics Technology Conference*, National United University, Miaoli, Taiwan, July 9-10, 2011.

[4] Black, R. J. and Moslehi, B. "Fiber Bragg Grating Interrogators for Structural Health Monitoring." *SAMPE 2008*. Long Beach, CA, May 18-22, 2008. Society for the Advancement of Material and Process Engineering. Paper 53-219. CD-ROM—9 pp.

[5] Moslehi, B., Black, R. J., Costa, J. M., Sotoudeh, V., and Faridian, F. "Highly scalable operational sensor system for harsh environment applications." *SAMPE 2012*. Baltimore, MD, May 21-24, 2012. Society for the Advancement of Material and Process Engineering. Paper 57-2333. CD-ROM—14 pp.

[6] Moslehi, B., Black, R. J., Costa, J. M., Edwards, E. H., Faridian, F., and Sotoudeh, V. "Fast fiber Bragg grating interrogation system with scalability to support monitoring of large structures in harsh environments." *Proc. SPIE* 9062. *SPIE Smart Structures and Materials+ Nondestructive Evaluation and Health Monitoring*, 2014. International Society for Optics and Photonics. pp. 906215-906215-12.

[7] Moslehi, B., Sotoudeh, V., Faridian, F., Costa, J. M., Black, R. J., Behbahani, A., O'Brien, W., Ha, D. S., and Austin, M. "Intelligent and robust sensors using fiber-optic network distributed engine control." *57th International Instrumentation Symposium*. St. Louis, Missouri, 2011. International Society of Automation. p. Vol. 488.

[8] Moslehi, B., Black, R. J., and Faridian, F. "Multifunctional Fiber Bragg Grating Sensing System for Load Monitoring of Composite Wings." *2011 IEEE Aerospace Conference*, Big Sky, MT, 2011, Paper 1557.

[9] Black, R. J., Chau, K., Chen, G., Moslehi, B., Oblea, L., and Sourichanh, K. "Optical

fiber gratings for structural health monitoring in high-temperature environments." *Proc. SPIE Sensor Systems and Networks - Phenomena Technology and Applications for NDE and Health Monitoring*, 2007. International Society for Optics and Photonics. p. 653001P.

[10] Chan, T. H. T., Yua, L., Tam, H. Y., Ni., Y. Q., Liu, S. Y., Chung, W. H., and Cheng, L. K. "Fiber Bragg grating sensors for structural health monitoring of Tsing Ma bridge: Background and experimental observation." *Engineering Structures* 28 (2006): 648–659.

[11] Chang, F.-K. Structural Health Monitoring 2009 – Proc. 7th International Workshop on Structural Health Monitoring. Lancaster, PA: DEStech Publications, 2009.

[12] Tennyson, R. C., Mufti, A. A., Rizkalla, S., Tadros, G., and Benmokrane, B. "Structural health monitoring of innovative bridges in Canada with fiber optic sensors." *Smart Materials and Structures* 10 (2001): 560–573.

[13] Todd, M. D., Johnson, G. A., and Vohra, S. T. "Deployment of a fiber Bragg grating-based measurement system in a structural health monitoring application,." *Smart Materials and Structures* 10 (2001): 534–539.

[14] Todd, M. D., Nichols, J. M., Trickey, S. T., Seaver, M., Nichols, C. J., and Virgin, L. N. "Bragg grating-based fibre optic sensors in structural health monitoring." *Philosophical Transactions of the Royal Society A: Mathematical, Physical and Engineering Sciences* 365 (2007): 317-343.

[15] Black, R. J., Costa, J. M., Moslehi, B., Zarnescu, L., Hackney, D., and Peters, K. "Fiber optic temperature profiling for thermal protection heat shields." *SPIE Smart Structures and Materials + Nondestructive Evaluation and Health Monitoring. Proc. SPIE 9062 - Smart Sensor Phenomena, Technology, Networks, and Systems Integration*. San Diego, CA, 2014. International Society for Optics and Photonics. San Diego, CA, 2014, pp. 906204-1 - 906204-12.

[16] Chau, K. K., Moslehi, B., Song, G., and Sethi, V. "Experimental demonstration of fiber Bragg grating strain sensors for structural vibration control." *SPIE Smart Structures and Materials - Proc. SPIE. 5391 - Sensors and Smart Structures Technologies for Civil, Mechanical, and Aerospace Systems*. San Diego, CA, March 14, 2004. International Society for Optics and Photonics. pp. 753-764.

[17] Nichols, J. M., Seaver, M., Trickey, S. T., Scandell, K. C., and Salvino, L. "Fiber Optic Strain Sensors (FOSS) to Monitor Strains on a Navy Vessel During Operations." *DTIC Document*, 2007.

[18] Seaver, M., Trickey, S. T., and Nichols, J. M. "Strain measurements from FBGs embedded in rotating composite propeller blades." *Optical Fiber Sensors*. Cancun, Mexico, October 23, 2006. Paper ThD2.

[19] Majewska, K., Mieloszyk, M., Ostachowicz, W., and Król, A. "Experimental method of strain/stress measurements on tall sailing ships using Fibre Bragg Grating sensors." *Applied Ocean Research* 47 (2014): 270-283.

[20] Yunxiang, Z., Ruquan, M., and Jingfeng, F. "Application of Fiber Bragg Grating Sensor for Stress Monitoring on Ship." *Transportation Science & Technology* 3 (2013): 055.

[21] Hess, P. "Structural health monitoring for high-speed naval ships." *7th International Workshop on Structural Health Monitoring*, Stanford, CA, 2007.

[22] Costa, J. M., Black, R. J., Moslehi, B., Oblea, L., Patel, R., Sotoudeh, V., Abouzeida, E., Quinones, V., Gowayed, Y., Soobramaney, P., and Flowers, G. "Fiber-optically sensorized composite wing." *SPIE Smart Structures and Materials+ Nondestructive*

Evaluation and Health Monitoring - Proc. SPIE 9062. San Diego, CA, 2014. International Society for Optics and Photonics—pp. 906213 - 906213-6.

[23] Nicolas, M., Sullivan, R. W., and Richards, W. L. "Fiber Bragg Grating Strains to obtain Structural Response of a Carbon Composite Wing." *ASME 2013 Conference on Smart Materials, Adaptive Structures and Intelligent Systems (SMASIS)*. Snowbird, Utah, 2013.

[24] Cusano, A., Capoluongo, P., Campopiano, S., Cutolo, A., Giordano, M., Felli, F., Paolozzi, A., and Caponero, M. "Experimental modal analysis of an aircraft model wing by embedded fiber Bragg grating sensors." *Sensors Journal, IEEE* 6 (2006): 67-77.

[25] Costa, J. M., Black, R. J., Moslehi, B., and Behbahani, A. R. "Advances in high temperature fiber optic sensors for turbine engine applications." *58th International Instrumentation Symposium (IIS).* San Diego, CA, 2012.

[26] Black, R. J., Chau, K., Good, L. K., Hernandez, M., Oblea, L., and Moslehi, B. "Fiber-Optic Sensing for Thermal Protection Structures in Vehicle Health Monitoring." *Proc. Quantitative Non Destructive Evaluation (QNDE)*, 2005.

[27] Black, R. J., Moslehi, B., Oblea, L., Yankelevich, D., Zare, D., Sathish, S., Schehl, N., Jata, K., and Neslen, C. "Fiber Bragg Gratings for Crack Growth and Thermal Monitoring." *SAMPE 2008. Long Beach, CA, May 18-22, 2008. Society for the Advancement of Material and Process Engineering.* Paper 53-060, 16 pp.

[28] Hackney, D. A., Peters, K. J., Black, R. J., Costa, J. M., Moslehi, B., and Zarnescu, L. "Fiber Bragg Gratings for Heat Flux Measurements in Thermal Protection Systems Under a Steady Conductive Thermal Load." *ASME 2013 Conference on Smart Materials, Adaptive Structures and Intelligent Systems*, 2013, pp. V002T05A009-V002T05A009.

[29] Black, R. J. and Moslehi, B. "Fiber Optic Sensors for Space." *Advances in Structural Health Monitoring of Space Systems*. Eds. A. N. Zagrai and D. Doyle. John Wiley & Sons, 2015.

[30] Park, Y.-L., Ryu, S. C., Black, R. J., Chau, K., Moslehi, B., and Cutkosky, M. R. "Exoskeletal Force Sensing End-Effectors with Embedded Optical Fiber Bragg Grating Sensors." *IEEE Trans. Robotics* 25 (2009): 1319-31.

[31] Moslehi, B., Black, R. J., Costa, J. M., Faridian, F., and Talnagi, J. "On-Line Monitoring of Flow-Accelerated Corrosion for Nuclear Power Plants." *U.S. Department of Energy* DOE/SC0004650-1, 2011.

[32] Sotoudeh, V., Moslehi, B., and Black, R. J. "Advanced Fiber Optic Condition Monitoring System for the Entire Wind Turbine Life Cycle." *Proc. OSA-MIT Topical Meeting on Optics and Photonics for Advanced Energy Technology*, Cambridge, MA, 2009, p. ThC2

[33] Bang, H.-J., Shin, H.-K., and Ju, Y.-C. "Structural health monitoring of a composite wind turbine blade using fiber Bragg grating sensors." *SPIE Smart Structures and Materials+ Nondestructive Evaluation and Health Monitoring*, 2010, pp. 76474H-76474H-12.

[34] Schroeder, K., Ecke, W., Apitz, J., Lembke, E., and Lenschow, G. "A fibre Bragg grating sensor system monitors operational load in a wind turbine rotor blade." *Measurement Science and Technology* 17 (2006): 1167.

[35] Sotoudeh, V., Moslehi, B., Black, R. J., Oblea, L., Chen, G., and Randles, P. W. "Fiber Bragg Grating Arrays for Impact Damage Monitoring in Concrete." *Proc. CONSEC'10 - Sixth International Conference on Concrete under Severe Conditions – Performance*

under Severe Loading. Mérida, México, 2010.

[36] Rodrigues, C., Félix, C., Lage, A., and Figueiras, J. "Development of a long-term monitoring system based on FBG sensors applied to concrete bridges." *Engineering Structures* 32 (2010): 1993-2002.

[37] Park, Y. L., Black, R. J., Moslehi, B., Cutkosky, M., Elayaperumal, S., Daniel, B., Yeung, A., and Sotoudeh, V. "Steerable Shape Sensing Biopsy Needle and Catheter." US Patent 8,649,847, February 11, 2014. U.S. Patent Application filed Sept. 18, 2009 and assigned PTO serial number 12/562,855; Provisional Patent Application 61/175,399 filed May 4, 2009.

[38] Park, Y.-L., Elayaperumal, S., Daniel, B., Ryu, S. C., Shin, M., Savall, J., Black, R. J., Moslehi, B., and Cutkosky, M. R. "Real-Time Estimation of Three-Dimensional Needle Shape and Deflection for MRI-Guided Interventions." *IEEE/ASME Trans. Mechatronics - Focused Section on Surgical and Interventional Medical Devices* 15 (2010): 906-915.

[39] Wright, P. J. The Future of Fiber Optics in the Offshore Oil Industry - http://www.odi.com/ODI_Documents/Articles_and_Papers/word_doc/Future%20of%20Fiber%20Optics.doc.

[40] Yamate, T. "Fiber optic sensors for the exploration of oil and gas." 19th International Conference on Optical Fibre Sensors – Perth, Australia – *Proc. SPIE* 7004 (2008)

[41] Zhang, Y., Ning, J., Li, S., Yin, Z., Chen, B., and Cui, H.-L. "Fiber-Bragg-grating-based seismic geophone for oil/gas prospecting." *Optical Engineering* 45 (2006): 084404 - 084404-4.

[42] Normann, R., Weiss, J., and Krumhansl, J. "Development of fiber optical cables for permanent geothermal wellbore deployment." *26th Workshop on Geothermal Reservoir Engineering*. Stanford University, Stanford, CA, 2001.

[43] Friebele, E. J., et al. "Optical fiber sensors for spacecraft applications." *Smart Mater. Struct.* 8 (1999): 813–838.

[44] Kang, H. K., Park, J. W., Ryu, C. Y., Hong, C. S., and Kim, C. G. "Development of fibre optic ingress/egress methods for smart composite structures." *Smart Mater. Struct.* 9 (2000): 149.

[45] Volanthen, M., Rumsey, L., Caesley, R., Ghoshal, A., Walsh, G., and Bordick, N. "The Embedding of Optical Fibre Sensors for SHM." *2009 SAMPE Fall Technical Conference*. Witchita, KA., Oct 19-22, 2009.

[46] Perez, I. M., Cui, H., and Udd, E. "Acoustic emission detection using fiber Bragg gratings." *SPIE's 8th Annual International Symposium on Smart Structures and Materials*, 2001. pp. 209-215.

[47] Sause, M. G. "Investigation of pencil-lead breaks as acoustic emission sources." *Journal of Acoustic Emission* 29 (2011): 184-196.

[48] Hsu, N. and Breckenridge, F. "Characterization and calibration of acoustic emission sensors." *Materials Evaluation* 39 (1981): 60-68.

[49] Sotoudeh, V., Black, R. J., Moslehi, B., and Qiao, P. "Lamb wave-based damage detection of composite shells using high-speed fiber-optic sensing." *SPIE Smart Structures + NDE*. San Diego, CA, March 2014, p. Paper 42.

[50] Black, R. J., Costa, J. M., Faridian, F., Moslehi, B., Pakmehr, M., Schlavin, J., Sotoudeh, V., and Zagrai, A. "Optical feather and foil for shape and dynamic load sensing of critical flight surfaces." *SPIE Smart Structures and Materials+ Nondestructive Evaluation and Health Monitoring*, 2014, pp. 90642S-90642S-8.

[51] Schlavin, J., Zagrai, A., Clemens, R., Black, R. J., Costa, J., Moslehi, B., Patel, R., Sotoudeh, V., and Faridian, F. “Combined electromechanical impedance and fiber optic diagnosis of aerospace structures.” *SPIE Smart Structures and Materials+ Nondestructive Evaluation and Health Monitoring*, San Diego, CA, 2014. International Society for Optics and Photonics pp. 90640X - 90640X-13.

[52] Zagrai, A. N. and Giurgiutiu, V. “Electro-mechanical impedance method for crack detection in thin plates.” *Journal of Intelligent Material Systems and Structures* 12 (2001): 709-718.